Minimum Threshold for Incipient Plasticity in the Atomic-Scale Nanoindentation of Au(111)

William Paul, David Oliver, Yoichi Miyahara, and Peter H. Grütter

Department of Physics, Faculty of Science, McGill University, Montreal, Quebec, Canada H3A 2T8

(Received 14 November 2012; published 27 March 2013)

The formation of the smallest permanent indentation in a Au(111) surface is studied by scanning tunneling microscopy and atomic force microscopy in ultrahigh vacuum. The 9.5 nm radius W(111) indenter was characterized *in situ* by field ion microscopy. Elastic and plastic indentations are identified both in the residual impression image and by features in their force-displacement curves such as the sink-in depth, pop-ins, and hysteresis energy. Plasticity is best identified quantitatively in the force-displacement curves by the sink-in depth. The minimum of plastic damage producible in the substrate is associated with an energy budget of ~70 eV.

DOI: 10.1103/PhysRevLett.110.135506 PACS numbers: 62.25.−g, 46.55.+d, 68.37.Ef, 68.37.Ps

Understanding the initial plastic yield of materials at the atomic scale is of fundamental importance for the design of new nanostructured materials [1] and elucidating the origins of wear and friction [2,3]. The onset of plasticity is commonly studied in nanoindentation, where the tip of a hard indenter is pressed into a sample material while the force and displacement are recorded simultaneously [4,5]. While the load is ramped at a constant rate, a sudden displacement burst, or ''pop-in'' is often observed, which is typically interpreted as the onset of plasticity.

Recent nanoindentation experiments inside a transmission electron microscope have shown that plastic deformation may in fact occur before the first obvious displacement burst is measured in the force-displacement curve [6]. In these, and many other nanoindentation experiments, the nucleation of the first dislocation is assumed to occur homogeneously within the material when the magnitude of the shear stress within the deformed volume approaches the theoretical shear strength of the material [7–10].

Schuh *et al.* inferred from variable loading rate and temperature experiments that dislocation nucleation is rate limited by a low energy barrier and has an activation volume on the size scale of a point defect [11]. Their quantitative analysis showed that the initiation of plasticity involves heterogeneous nucleation sites. More recently, Wagner *et al.* studied the effects of finite temperature and atomic-scale indenter roughness on the dislocation nucleation in multiscale atomistic simulations [12]. Their picture of the first plastic event in Al(111) at 300 K is also a heterogeneous one and involves thermally generated transient ''hot-spot'' defects that decrease the load required to initiate plastic deformation.

An interesting fundamental question in the atomistic understanding of plasticity is the minimum stable defect configuration when a single crystal is indented, that is, the smallest possible ''quantum'' of plasticity producible by indentation. Here, we investigate incipient plasticity in atomic-scale indentation on a single crystal and measure a clear but stochastic transition from elastic loading to plastic indentation of a contact. These indentations at the threshold of plasticity correspond to the smallest permanent damage that can be produced in the substrate and we quantify the scale of this minimum deformation. We find evidence that incipient plasticity is indeed an activated process involving heterogeneous nucleation sites. We observe that pop-ins in the force-displacement curve are correlated with incipient plasticity, but that other quantitative indicators provide a better diagnostic of plasticity, which is relevant in the context of applications such as nanomachining by indentation [13].

Compared to traditional nanoindentation, our experiment offers excellent force resolution down to the nano-Newton regime, making it possible to capture the earliest indications of plasticity in force-displacement curves. The indentation depth is also precisely determined, which is not possible in traditional atomic force microscope (AFM) indentation due to problems with quantitative beam deflection calibration and large piezo displacements causing creep and hysteresis. Our AFM-based indentation is not affected by these issues because of its interferometric detection method where displacements are directly calibrated to the wavelength of laser light and relatively small piezo displacements ensure minimal piezo hysteresis.

The initial plastic damage to a Au(111) single crystal has been investigated by combined scanning tunneling microscopy (STM) and AFM, where our indenter, a W(111) single crystal tip, was characterized on the atomic scale by field ion microscopy (FIM). The exceptional spatial resolution of STM allows the indentation sites to be imaged after the experiment, determining the presence or absence of plastic deformation.

Experiments were carried out in ultrahigh vacuum (UHV) at room temperature. Au(111) substrates were prepared by epitaxial growth of Au, 100 nm thick, on a $\sim 1 \times 5$ mm piece of 50 μm thick mica. The Au(111) surface was cleaned by repeated 1 keV Ne^+ ion sputtering and annealing cycles in UHV. The mica beam was cantilevered, such that it could deflect upon interaction with the tip. Forces were

extracted by monitoring the cantilever's deflection by interferometry [14]. Indentations were performed at the location where the sample's spring constant was 200 ± 20 N/m. This uncertainty limits the absolute force accuracy to ~10%. During indentation experiments, the conductance of the junction was recorded simultaneously with the load over the tunneling to contact range (pA to μA) using a logarithmic current preamplifier [15].

The indenter consists of a tip electrochemically etched from W(111) wire and prepared by flash annealing and degassing cycles in UHV [16,17]. Field evaporation of adsorbates in FIM yields a clean W(111) tip ending in a 9.5 ± 1.1 nm radius spherical apex, as determined by the ring counting method [18,19]. A FIM image of the tip apex is shown in Fig. 1(a), where the atoms of the highly corrugated (111) plane are individually resolved.

A constant-current STM topograph of the Au(111) surface is shown in Fig. 1(c). The herringbone reconstruction is faintly resolved as rows running parallel to the $(11\bar{2})$ direction. The area of the sample in which indentations were carried out is an atomically flat Au(111) terrace: a 0.24 nm atomic step is visible at the bottom right corner of the image, and several steps occur at the top of the image. After the STM scan, the tip was moved under constant-current feedback at 20 pA and -0.05 V sample bias to the site of each indentation using the Raster Probe control of GXSM to create a 5×5 array of indentations [20]. At each location of the array, the tip was retracted to -2 nm from the tunneling setpoint and then approached toward the sample at a speed of 2 nm/s to $+2$ nm beyond the tunneling setpoint (loading). The tip was then retracted (unloading).

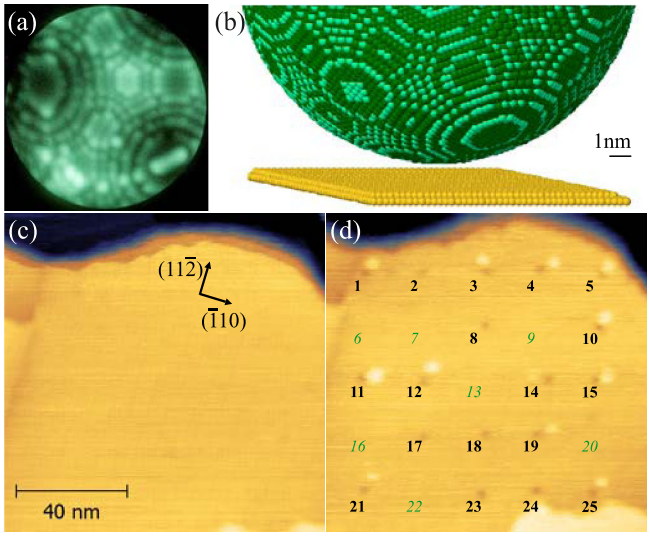

FIG. 1 (color online). (a) FIM image of the W(111) indenter (5.5 kV tip voltage); (b) ball model of a W(111) with a 9.5 nm radius and Au(111) substrate to scale; (c) Au(111) terrace before and (d) after a 5×5 indentation array with 20 nm spacing between indents (20 pA, -0.05 V sample bias). Bolded numbers indicate plastic sites; italicized numbers indicate elastic sites.

The indentation depth was chosen to be close to the minimum threshold for observing plastic deformation of the substrate. The actual penetration depth for these indentations is less than 2 nm due to the simultaneous deflection of the cantilevered sample and varies with the elastic or plastic characteristics of each indentation.

The indentations were made in the numbered order indicated on the STM topograph of Fig. 1(d)). The elastic indentations (where no residual impression is imaged) are numbered in italics. Although the maximum force at each indentation site is very similar, plasticity is not always initiated due to the fact that it is an activated process.

The plasticity visible in the indentation array corresponds to the smallest permanent damage that can be made by indentation of the Au(111) surface just beyond elastic loading. This damage is stable over many STM scans, indicating that the undamaged regions were not repaired by thermally diffusing Au adatoms or vacancies before they could be imaged. A single atomic layer of pileup next to the indentation site is observed in many cases.

A striking correspondence between the imaged surface damage in STM and the features of the force-displacement curves is observed. Figure 2 presents illustrative force-displacement curves from the array produced in Fig. 1(d). The depth axis is zeroed to the crossing of the 1 GΩ tunneling gap resistance upon loading.

Two of the elastic indentation curves are plotted in Figs. 2(a) and 2(b). At zero depth, the tunneling current has reached 50 pA, and rises exponentially through the tunneling regime. At ~0.75 nm, the force becomes repulsive and smoothly increases to a maximum of ~130 nN where the conductance of the junction is ~22 G_0 (where $G_0 = 2e^2/h$ is the conductance quantum).

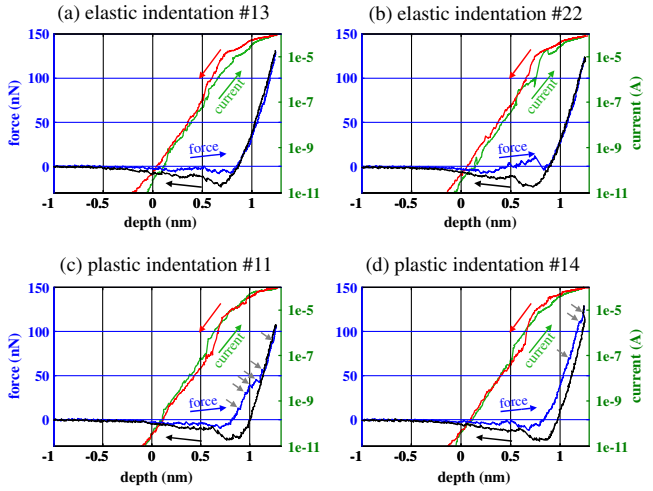

FIG. 2 (color online). Force and current recorded during indentation at elastic sites, (a) and (b), and plastic sites, (c) and (d). Loading and unloading directions are indicated by arrows. Additional arrows in (c) and (d) point to pop-in discontinuities in the force.

Upon retraction, the unloading force curve overlaps the loading curve closely. The elastic indentations have characteristically well-overlapping loading and unloading curves and generally an absence of pop-ins in the repulsive force region (sometimes small pop-ins are observed as discussed later). A reduced elastic modulus of 92 ± 12 GPa is extracted from an Oliver-Pharr [21] analysis of the unloading curves using the known 9.5 nm tip radius from FIM. This agrees well with the expected combined modulus [22] of 80 GPa for a W-Au contact.

Despite the fact that no substrate damage occurs in the elastic sites, we observe a significant and variable hysteresis in the low load region of their force-displacement curves. We attribute this variability to the compression and rearrangement of Au on the tip which is picked up during indentation and scanning (see Supplemental Material [23]). The indentation only enters the strongly repulsive regime at about 0.75 nm depth after the soft Au layers on the tip have rearranged. We refer to the initial portion of the curve as the "tip rearrangement" region.

The indentations corresponding to plastic sites show multiple pop-ins as a signature of plasticity. Pop-ins are characterized by an instantaneous reduction in force and a simultaneous increase in penetration depth—these quantities are linked by the ~ 200 N/m stiffness of the force transducer. In the plastic indentations of Figs. 2(c) and 2(d), pop-ins are indicated by arrows pointing to the sudden jumps in the force curve at 14, 32, 41, 46, 58, and 89 nN and 71, 115, and 123 nN, respectively. The last pop-in in Fig. 2(d) occurs in the unloading curve. Reverse plasticity in the form of pop-outs is not observed; however, it has been observed in similar experiments performed to much higher loads [24]. Changes in junction conductance sometimes occur simultaneously with pop-ins in the force channel (not shown).

We now consider several indicators derived from the force-displacement data and compare them with the evidence of plasticity from STM imaging. The first is the hysteresis energy, obtained by integrating the force over the excursion of the indentation. In Fig. 3(a), the circled points correspond to elastic sites and show a large variability due to the details of the tip rearrangement region. The elastic sites have an average hysteresis energy of 46 ± 20 eV. The quoted error is the standard deviation of the measured values and does not take into account the $\sim 10\%$ systematic uncertainty in the force data. At the plastic sites, the measured hysteresis energies are all substantially larger with an average of 117 ± 16 eV. Tip rearrangements also contribute to the scatter of the plastic hysteresis energies. The variability of the hysteresis energy due to tip rearrangements is well illustrated in the force-displacement curves in Figs. 2(a) and 2(b): both indentations are elastic but show very different hysteresis energies of 47 and 83 eV, respectively, due to the tip rearrangement region.

The hysteresis energy in the elastic sites gives a measure of the energy spent to irreversibly compress and extend Au

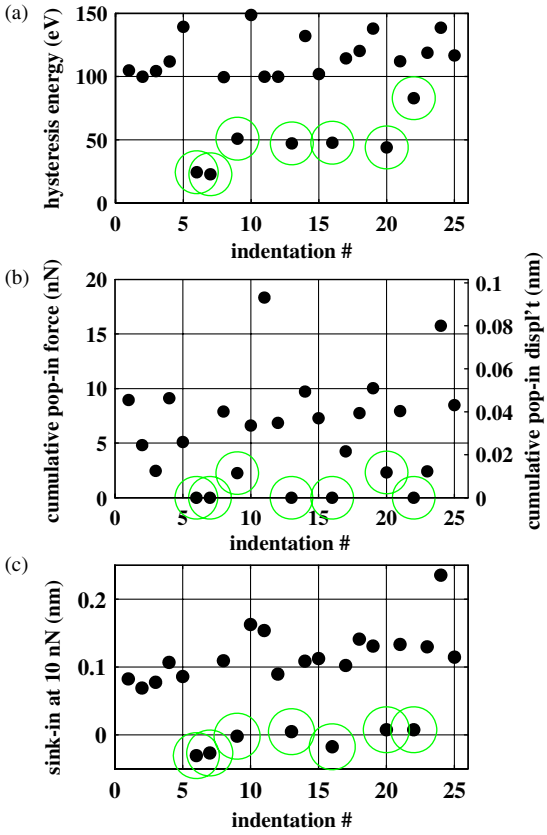

FIG. 3 (color online). (a) Hysteresis energy obtained by integrating force-displacement curves. (b) Cumulative pop-in force and displacement obtained by summing pop-in events in each curve. (c) Sink-in depth between loading and unloading curves at 10 nN. Elastic sites are indicated by additional circles.

adhering to the tip. Subtracting this average 46 eV from the 117 eV measured in the plastic sites suggests that ~ 70 eV is available for the creation of the dislocation loops and plastic damage in the sample. This energy corresponds to that of an edge dislocation threading ~ 12 atomic planes [25] or the energy required to break several tens of atomic bonds [26]. It is impossible to determine by STM if the damage consists of a subsurface dislocation or a vacancy cluster, but it can be concluded that this excess energy corresponds to some minimal defect configuration associated with permanent plasticity. Further advanced atomistic modeling is needed to understand the mechanisms and final atomic configurations of the defects involved.

The sum of all pop-in discontinuities in each force-displacement curve is plotted in Fig. 3(b). Pop-ins in the tip rearrangement region were not included in the sum. The cumulative displacement associated with these pop-ins, linked by the ~ 200 N/m sample stiffness, is shown on the right vertical axis. The cumulative pop-in displacement indicates the elastic or plastic nature of the indentations with an average of 0.003 ± 0.006 nm for the elastic sites and 0.04 ± 0.02 nm for the plastic sites. We note that discontinuities in displacement as small as ~ 0.01 nm are

detected, well below the minimum pop-in distance observed in previous studies [27,28]. These distances are far below the 0.24 nm Au(111) plane spacing, which may reflect the role of elastic recovery of the substrate after the pop-in.

Some elastic sites, indicated by additional circles, show a finite pop-in displacement. These small pop-ins may be due to the reversible nature of the first dislocation nucleation event [29], to tip rearrangements occurring at higher loads, or to reversible dislocation loops confined to the surface [12].

The indicator that was found to reflect most clearly the presence of plasticity is the sink-in depth measured at low repulsive load. This is the difference of the penetration depth where the loading and unloading curves cross a repulsive load of 10 nN (chosen to be above the load at which tip rearrangements occur). The sink-in depth, plotted in Fig. 3(c), is independent of the details occurring in the tip rearrangement region. The average sink-in depth is -0.01 ± 0.02 nm for the elastic sites and 0.12 ± 0.04 nm for the plastic sites. We suggest that the sink-in depth could be used as a reliable indicator of the creation of plastic damage in nanomachining applications.

An alternative sink-in depth calculated from the conductance (from any value in the range 0.01 to 10 G_0) does not serve as a reliable indicator of plastic damage due to tip rearrangements and wire formation (not shown).

Finally, we summarize the force at which the first pop-in occurs in Fig. 4 as a cumulative distribution. In order to consider a larger statistical ensemble, we add to this plot the data from the first pop-ins in another 50 indentations performed with the same tip-sample system but to higher loads. The force at which the first pop-in occurs reflects the shear stress in the sample at the onset of plasticity. The maximum shear stress in the elastic contact at the first yield point is estimated from the Hertz model [30]

$$\tau_{\max} = \left(\frac{0.56}{\pi}\right) F^{1/3} \left(\frac{E^*}{R}\right)^{2/3},$$

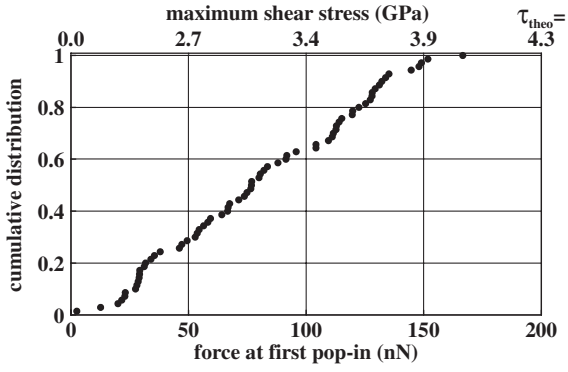

FIG. 4. Cumulative distribution of the force measured at the first pop-in and corresponding maximum shear stress calculated from the Hertz model.

where F corresponds to the force at the first pop-in, R is the tip radius determined by FIM, and E^* is the combined modulus for the W-Au contact of 80 GPa. The shear stress is shown on the top axis of Fig. 4.

In a picture of homogeneous nucleation, one expects that the maximum shear stress within the substrate at the yield point to be on the order of the theoretical shear stress of the material. For gold, this corresponds to a shear stress of about $G/2\pi \approx 4.3$ GPa, where G is the shear modulus [31]. It is apparent from the cumulative distribution that the first detected pop-in appears at highly variable loads with corresponding stresses that are in all cases much lower than the theoretical shear strength (at the right limit of the plot).

A transition between elastic and plastic behavior is clearly reflected both in STM images and in properties of the force-displacement curves. Other than to show that the homogeneous nucleation of dislocations does not occur in our system, we cannot determine the mechanisms governing the first pop-in or the initiation of plasticity.

In these experiments, the tip structure is known in exquisite detail from FIM, and a minimum energy of $\sim$70 eV has been found necessary to produce a minimum plastic deformation in Au(111), just above the threshold of elastic loading. The length scales of our experiment—including the indenter size—match those accessible in molecular dynamics modeling, inviting an atomistic understanding of the observed plasticity threshold. Can modeling reproduce the observed energy minimum? What is the origin of the minimum plastic energy? What atomistic processes take place during the plastic deformation, and what is the atomic configuration of the defect after plastic indentations? Furthermore, modeling would be a convenient manner to explore if a threshold between elastic and plastic loading is universal in other fcc (or bcc) metals, or for other crystallographic orientations of the substrate. Results from such studies would also provide a springboard for further experiments.

The effect of the atomic-scale surface roughness of the indenter, of increasing concern in recent modeling work [12,32], is directly accessible in our experiment as the exact crystal structure of the indenter is known. Heterogeneous nucleation of plasticity aided by surface roughness may well be plausible under the circumstance of extremely sharp tips where stress gradients are sufficiently large, and the maximal shear stress is concentrated only a few nm below the sample surface.

In summary, indentations resulting in the smallest permanent deformation of the Au(111) surface have been performed by combined AFM and STM using a well-defined W(111) indenter characterized by FIM. We find a clear correspondence between plasticity identified in STM images and characteristics of the force-displacement curves. This minimum deformation is associated with an energy budget of $\sim$70 eV. The best indication of plasticity

from the force-displacement data is found to be the sink-in depth measured at low repulsive load. We propose the utility of this parameter for determining plasticity from force-displacement curves alone, in contexts where imaging the surface is not possible or not practical.

The forces measured at the first pop-in event correspond to stresses much lower than the theoretical shear strength, suggesting that dislocations are not homogeneously nucleated within the bulk. Further modeling work would contribute to an understanding of the atomistic mechanisms involved in the threshold of plasticity and the final defect structures, the minimum plastic energy, and the ubiquitousness of the plasticity threshold in other materials.

The authors acknowledge NSERC, CIFAR, and RQMP for funding.

[1] R. Valiev, Nature (London) **419**, 887 (2002).
[2] M. Urbakh, J. Klafter, D. Gourdon, and J. Israelachvili, Nature (London) **430**, 525 (2004).
[3] B. Bhushan, J. N. Israelachvili, and U. Landman, Nature (London) **374**, 607 (1995).
[4] A. C. Fischer-Cripps, *Nanoindentation* (Springer, New York, 2011).
[5] M. F. Doerner and W. D. Nix, J. Mater. Res. **1**, 601 (1986).
[6] A. M. Minor, S. A. S. Asif, Z. Shan, E. A. Stach, E. Cyrankowski, T. J. Wyrobek, and O. L. Warren, Nat. Mater. **5**, 697 (2006).
[7] J. Li, K. J. Van Vliet, T. Zhu, S. Yip, and S. Suresh, Nature (London) **418**, 307 (2002).
[8] A. Gouldstone, K. J. Van Vliet, and S. Suresh, Nature (London) **411**, 656 (2001).
[9] S. N. Dub, Y. Y. Lim, and M. M. Chaudhri, J. Appl. Phys. **107**, 043510 (2010).
[10] P. Tangyunyong, R. C. Thomas, J. E. Houston, T. A. Michalske, R. M. Crooks, and A. J. Howard, Phys. Rev. Lett. **71**, 3319 (1993).
[11] C. A. Schuh, J. K. Mason, and A. C. Lund, Nat. Mater. **4**, 617 (2005).
[12] R. J. Wagner, L. Ma, F. Tavazza, and L. E. Levine, J. Appl. Phys. **104**, 114311 (2008).
[13] *Nanotribology and Nanomechanics II*, edited by B. Bhushan (Springer, New York, 2011).
[14] C. Schönenberger and S. F. Alvarado, Rev. Sci. Instrum. **60**, 3131 (1989).
[15] U. Dürig, L. Novotny, B. Michel, and A. Stalder, Rev. Sci. Instrum. **68**, 3814 (1997).
[16] T. Hagedorn, M. El Ouali, W. Paul, D. Oliver, Y. Miyahara, and P. H. Grütter, Rev. Sci. Instrum. **82**, 113903 (2011).
[17] A.-S. Lucier, MS thesis, McGill University, 2004.
[18] W. Paul, Y. Miyahara, and P. H. Grütter, Nanotechnology **23**, 335702 (2012).
[19] A.-S. Lucier, H. Mortensen, Y. Sun, and P. H. Grütter, Phys. Rev. B **72**, 235420 (2005).
[20] P. Zahl, T. Wagner, R. Moller, and A. Klust, J. Vac. Sci. Technol. B **28**, C4E39 (2010).
[21] W. C. Oliver and G. M. Pharr, J. Mater. Res. **19**, 3 (2004).
[22] A. C. Fischer-Cripps, *Introduction to Contact Mechanics* (Springer, Boston, 2007).
[23] See Supplemental Material at http://link.aps.org/supplemental/10.1103/PhysRevLett.110.135506 for additional experimental results pertaining to tip wetting.
[24] D. J. Oliver, J. Maassen, M. El Ouali, W. Paul, T. Hagedorn, Y. Miyahara, Y. Qi, H. Guo, and P. H. Grütter, Proc. Natl. Acad. Sci. U.S.A. **109**, 19 097 (2012).
[25] D. Hull and D. J. Bacon, *Introduction to Dislocations* (Elsevier, New York, 2011), 5th ed.
[26] G. S. Rohrer, *Structure and Bonding in Crystalline Materials* (Cambridge University Press, New York, 2001).
[27] T. Filleter, S. Maier, and R. Bennewitz, Phys. Rev. B **73**, 155433 (2006).
[28] P. Egberts and R. Bennewitz, Nanotechnology **22**, 425703 (2011).
[29] C. L. Kelchner, S. J. Plimpton, and J. C. Hamilton, Phys. Rev. B **58**, 11 085 (1998).
[30] K. L. Johnson, *Contact Mechanics* (Cambridge University Press, New York, 1996).
[31] W. Soboyejo, *Mechanical Properties of Engineered Materials* (Marcel Dekker, New York, 2003).
[32] B. Luan and M. O. Robbins, Nature (London) **435**, 929 (2005).